Dyes and Pigments 128 (2016) 41–48

Contents lists available at ScienceDirect

Dyes and Pigments

journal homepage: www.elsevier.com/locate/dyepig

G-quadruplex DNA interactions, docking and cell photocytotoxicity research of porphyrin dyes

Ping Zhao [a, *], Min-Chao Liu [a], Min Zheng [b, **], Shu-fang Jin [a], Ding-tong Tang [a], Jiong Chen [a], Yan-na Ma [a], Jia-qi Lin [a], Xia-hong Wang [a], Hong-jian Liu [a]

[a] School of Chemistry and Chemical Engineering, Guangdong Pharmaceutical University, No. 280, Waihuandong Road, Education Mega Centre, Guangzhou 510006, PR China
[b] School of Basic, Guangdong Pharmaceutical University, No. 280, Waihuandong Road, Education Mega Centre, Guangzhou 510006, PR China

ARTICLE INFO

Article history:
Received 24 November 2015
Received in revised form
5 January 2016
Accepted 7 January 2016
Available online 15 January 2016

Keywords:
Cationic porphyrins
G-quadruplex DNA
Spectral method
Molecular dock
Steric hindrance
Photocytotoxicity

ABSTRACT

5,10,15,20-tetra-(*N*-methyl-2-pyridyl)porphyrin ($TMPyP_2$) was always paid little attention because it has relatively low DNA-binding affinity and photocytotoxicity compared with its positional isomer 5,10,15,20-tetra-(*N*-methyl-4-pyridyl)porphyrin ($TMPyP_4$). Inspired by the previous successful results on higher bioactivities of ligands with larger aromatic surfaces, herein, 5,10,15,20-tetra (phenyl-4-N-methyl-2-pyridyl) porphyrin ($TPMPyP_2$), a $TMPyP_2$-like porphyrin with enlarged planar substituents, was designed and successfully synthesized. Results from spectral experiments and molecular docking calculation suggest that $TPMPyP_2$ could partially overcome the steric hindrance of $TMPyP_2$, with more favorable DNA-binding mode and lower molecular binding energy (M.B.E). Meanwhile, cell photocytotoxicity research indicates that $TPMPyP_2$ shows higher antitumor potency than $TMPyP_2$, which allowed the previous conclusion that the higher G-Quadruplexes DNA binding affinity would be related to better photocytotoxicity.

1. Introduction

It is well known that telomerase activity is needed for tumor cell proliferation and thus telomerase presents a potential selective target for the design of new antitumor drugs [1]. In the absence of an X-ray crystal structure of telomerase, the design of inhibitors that directly target telomerase is relatively difficult. An important approach would be to target the G-quadruplex (G4) DNA that has been proposed to be associated with the telomerase reaction cycle. It is frequently reported that G4-binding and G4-promoting small molecules can in principle effectively inhibit both the catalytic and capping functions of telomerase, which has been the driving force behind the investigation of ligands that stabilize G-quadruplexes and/or induce their formation (G4-ligands) [2,3].

G4-ligands including several porphyrin based compounds have been explored for their potential as anti-cancer drugs [4]. The porphyrin-based ligands have shown the ability to inhibit telomerase and they typically exhibit low cytotoxicity. 5,10,15,20-(N-methyl-4-pyridyl) porphyrin ($TMPyP_4$) has been intensively used as a model ligand in the characterization of the structure, stability, and ligand binding properties of oncogene promoter sequence G-quadruplexes [5].

Although $TMPyP_4$ is intensively studied for the excellent performance on G4-binding and photocytotoxicity, its positional isomer, 5,10,15,20-(N-methyl-2-pyridyl) porphyrin ($TMPyP_2$) tell us a quite different story with much lower G4-binding activity and 10-fold higher IC_{50} value of photocytotoxicity [6,7]. For $TMPyP_2$, due to the steric repulsion between the 2-methyl groups in the pyridyl rings and the β-hydrogens in the porphine core, there may be a high-energy barrier for the pyridyl rings to become coplanar with the porphine. Furthermore, the methyl groups on the pyridine rings of $TMPyP_2$ lie partially over the face of the porphyrin ring, posing a π−π stacking interaction and also increasing the thickness of $TMPyP_2$ which hinder the intercalation of $TMPyP_2$ into the G4-DNA structure. Thus, the efforts on improving $TMPyP_2$-like porphyrins were relatively rare.

Based on the former successful research on polypyridine, anthraquinones and phenanthrolines, which suggested that extended aromatic surfaces always do favors to the drug−DNA interactions

* Corresponding author. Tel./fax: +86 760 88207939.
** Corresponding author. Tel.: +86 20 39352187; fax: +86 20 39352186.
E-mail addresses: zhaoping666@163.com (P. Zhao), sourcabage@126.com (M. Zheng).

http://dx.doi.org/10.1016/j.dyepig.2016.01.009
0143-7208/

[8–12], we supposed that designing porphyrins with extended planar substituents would bring us new surprising on the discovery of ligands with higher biochemical abilities. In this paper, 5,10,15,20-tetra (phenyl-4-N-methyl-2-pyridyl) porphyrin ($TPMPyP_2$, see molecular structure in Fig. 1), a $TMPyP_2$-like porphyrin with enlarged planar substituents, was successfully synthesized and comparatively studied with $TMPyP_2$. We have compared their interactions with a guanine quadruplex DNA, 5′-$AG_3T_2AG_3T_2AG_3T_2AG_3$-3′ (AG22, see Schematic diagram in Fig. 2), by using surface-enhanced Raman spectroscopy (SERS), emission, absorption, Induced circular dichroism (ICD), FRET melting assay experiment in combination with molecular docking calculation. The photocytotoxic activities of these two porphyrins were evaluated by WST assay, cell cycle analysis and morphological change methods.

2. Experimental

2.1. Synthesis

Classical Adler–Longo method [13] was used to synthesize the porphyrins, and the synthetic pathway was given in Fig. 1. A mixture of propionic acid, acetic anhydride and corresponding aldehyde was heated at 130 °C with stirring. Appropriate aryl carboxaldehyde and pyrrole were then added separately from dropping funnels to the refluxing mixture. The resulting mixture was refluxed for 1.5 h. The solvent was subsequently evaporated under reduced pressure. The residue was then purified by column chromatography. Methylation by an excess amount of methyl iodide afforded target compounds.

The spectroscopic results obtained from 5,10,15,20-tetra (phenyl-4-N-methyl-2-pyridyl) porphyrin ($TPMPyP_2$): ^{1}H NMR (500 MHz, DMSO) δ: 9.26 (d, J = 9.2 Hz, 4H), 8.63 (d, J = 6.0 Hz, 4H), 8.38 (d, J = 7.8 Hz, 4H), 7.83 (d, J = 6.4 Hz, 8H), 7.36 (d, J = 6.8 Hz, 16H), 4.42 (s, 12H), −2.8 (s, 2H). ^{13}C NMR (500 MHz, DMSO): δ 46.77, 119.26, 121.29, 127.03, 129.45, 130.60, 132.17, 132.41, 132.77, 134.18, 134.40, 144.90, 145.25, 149.20, 150.04, 180.73, 181.85. ES-MS [EtOH–$CHCl_3$, m/z]: 245 ($[M-4I]^{4+}$), 327($[M-4I]^{3+}$), 491($[M-4I]^{2+}$), 982($[M-4I]^{+}$). Anal. Calcd for $C_{68}H_{54}N_8I_4\cdot 3H_2O$: C, 52.87; H, 3.91; N, 7.25. Found: C, 53.09; H, 4.04; N, 7.36. UV–Vis (10 μM in Tris buffer), λ_{max} (nm) (log ε): 419(4.21), 508(3.19), 558(3.37), 567(3.08), 631(2.22).

The spectroscopic results obtained from 5,10,15,20-tetra (N-methyl-2-pyridyl) porphyrin ($TMPyP_2$): ^{1}H NMR (500 MHz, DMSO): chemical shift δ: chemical shift δ: 9.51 (d, J = 9.2 Hz, 4H), 9.24 (d, J = 9.6 Hz, 4H), 8.92 (d, J = 7.2 Hz, 8H), 8.87 (d, J = 6.4 Hz, 8H), 8.36 (d, J = 7.8 Hz, 8H), 4.44 (s, 6H), −2.13 (s, 2H). ^{13}C NMR (500 MHz, DMSO): δ 47.90, 116.29, 123.98, 124.49, 125.55, 129.36, 131.83, 136.37, 137.55, 145.90, 147.51, 151.15, 153.88, 154.30. ES-MS [EtOH–$CHCl_3$, m/z]: 169 ($[M-4I]^{4+}$), 226($[M-4I]^{3+}$), 339($[M-4I]^{2+}$), 678($[M-4I]^{+}$). Anal. Calcd for $C_{44}H_{38}N_8I_4\cdot 4H_2O$: C, 41.99; H, 3.68; N, 8.90. Found: C, 42.11; H, 3.87; N, 8.98. UV–Vis (10 μM in Tris buffer), λ_{max} (nm) (log ε): 421(4.73), 515(3.19), 563(3.58), 578(3.12), 618(2.82).

The ^{1}H NMR, ^{13}C NMR and Mass spectrum are given as supplemental information in Figs. S1–S3.

2.2. Materials

The HPLC-purified DNA oligonucleotides were purchased from the Shanghai Sangon Biological Engineering Technology & Services Co., Ltd. (China). The single-strand extinction coefficient was calculated by Nearest-neighbor approximation method [14], using extinction coefficients at 260 nm of 228, 500 M^{-1} cm^{-1}.

The formation of intra- and inter-molecular G-quadruplexes was carried out as follows: the oligonucleotide sample 5′-$AG_3T_2AG_3T_2AG_3T_2AG_3$-3′ (AG22) or fluorescent-labeled oligonucleotide sample 5′-FAM-$G_3T_2AG_3T_2AG_3T_2AG_3$-TAMRA-3′ (F21T, FAM: 6-carboxyfluorescein, TAMRA: 6-carboxytetramethylrhodamine), was dissolved in a Tris buffer solution (consisting of 10 mM Tris–HCl, 1 mM Na_2EDTA, and 100 mM NaCl, pH 7.4) for AG22 or a PBS buffer (consisting of 10 mM K_2HPO_4/KH_2PO_4, 40 mM KCl, 100 mM NaCl, pH 7.4) for F21T. Then the solution was heated to 90 °C for 5 min, gently cooled to room temperature, and then incubated at 4 °C overnight. The formation of G4-DNA was affirmed by the appearance of positive peak near 290 nm and negative trough near 265 nm in CD spectra, which is characteristic of antiparallel-stranded G-quadruplexes [14].

2.3. Instruments and methods

UV–Vis spectra were recorded on a Hitachi U-3900H spectrophotometer. Induced circular dichroism (ICD) spectra were recorded on a JASCO-J810 spectrometer. FRET spectra and FRET melting assay experiments were recorded on a Sanco 970CRT spectrofluorophotometer. FRET melting assay was conducted on Perkin–Elmer Ls55 spectrofluorophotometer with a temperature controller. Cell viability assay was performed with a microplate reader (model 680, Bio-Rad, USA). Cell cycle analysis, annexin V–fluorescein isothiocyanate/propidium iodide (PI) assay of apoptotic cells and detection of mitochondrial membrane potential were performed with a FACS can flow cytometer (BD, USA). Fluorescence microscopy of apoptosis assays was performed with an OX31 fluorescence microscope (Olympus, Japan). Data were expressed as the mean ± the standard deviation from three independent experiments. Statistical analysis was performed using origin 8.0. Comparisons between two groups were performed by an unpaired t test. Multiple comparisons between more than two groups were performed by one-way analysis of variance. Significance was accepted at a P value lower than 0.05.

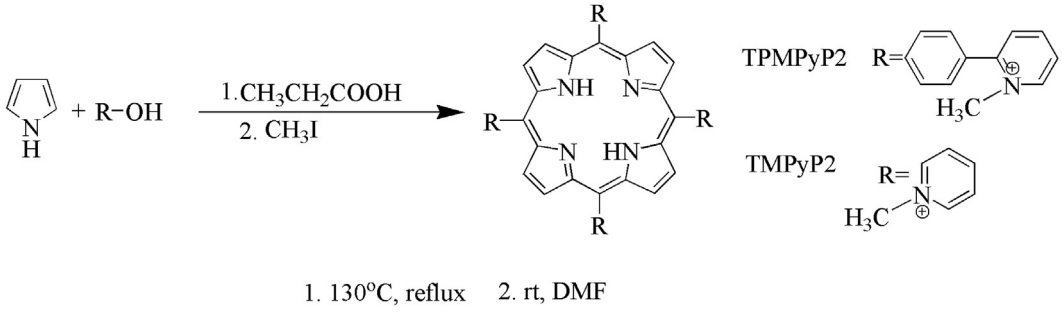

Fig. 1. The synthetic pathway of $TMPyP_2$ and $TPMPyP_2$.